圧電MEMS型波長可変VCSELによる線形掃引と高速変調

Piezoelectric Tunable MEMS-VCSEL for Linear Sweep and High-Frequency Modulation

奥村　聡* 泉谷　一磨* 藤島　正幸* 坂井　篤* 軸谷　直人*
So OKUMURA Kazuma IZUMIYA Masayuki FUJISHIMA Atsushi SAKAI Naoto JIKUTANI

要　旨

周波数連続変調方式（FMCW）LiDARはレーザー光の波長を連続的に変調することで，direct time-of-flight（dToF）方式より高精度な測距を可能とする．しかし，連続波長掃引の非線形性や中心波長の設計値からのずれによる分解能の悪化や，低い波長掃引周波数によるフレームレートの低下などの課題がある．そこで我々は，電圧に対する体積変化の線形応答と高い圧電定数を有するチタン酸ジルコン酸鉛（PZT）からなる圧電素子を用いた微小電子機械システム（MEMS）と，垂直共振器型面発光レーザー（VCSEL）とを組み合わせた初の圧電MEMS型波長可変VCSEL (MEMS-VCSEL) を提案し，光源単独で中心波長調整の高い線形性と高い周波数での掃引が可能なFMCW LiDAR用光源の実現を目指した．MEMSチップの中心部に膜構造を，外周部には蛇腹構造を設け940 nm帯のhalf-VCSELチップと熱圧着で接合した．その結果，蛇腹構造のDC電圧駆動により決定係数0.99以上の高い線形性で中心波長を制御し，膜構造の1.3 MHzの共振周波数により2.98 nmの連続波長掃引幅を持つ波長可変光源を実現した．この変調周波数はDBR型MEMS-VCSELの報告例の中で最も高く，高速動作を実現した．

ABSTRACT

Frequency modulated continuous wave (FMCW) provides more accurate ranging than direct time-of-flight by continuously modulating laser wavelength. However, there are issues such as deteriorated resolution due to the nonlinearity of the wavelength sweep and the deviation of the center wavelength from the designed value, and limited frame rate resulting from the low-frequency sweep. We propose piezoelectric MEMS-VCSEL which consists of micro electro mechanical system (MEMS) using $Pb(Zr_xTi_{1-x})O_3$ (PZT) with a high piezoelectric constant and linear response of volume change to the applied voltage, and a vertical-cavity surface-emitting laser (VCSEL) for the first time. We aim for high linearity in the center wavelength tuning and a high sweep frequency using the chip itself for a compact laser source of FMCW LiDAR. The meander structure at the outer periphery and membrane structure at the center of the MEMS are implemented. The MEMS and 940-nm half-VCSEL are combined by thermal bonding. The resulting MEMS-VCSEL achieved high linearity in the center wavelength tuning with a coefficient of determination over 0.99 under DC-voltage actuation of the meander structure. The continuous wavelength tuning range reached 2.98 nm with a resonant frequency of the membrane at 1.3 MHz. This sweep frequency is the highest among DBR MEMS-VCSELs and enabled fast operation.

* リコー 先端技術研究所　HDT研究センター
Ricoh, Advanced Techonology R&D Division, Human Digital Twin Institute

本稿はSPIE (Society of Photo-Optical Instrumentation Engineers) の以下の論文を基に許諾を受けて作成した．
S. Okumura et al.: PZT MEMS-VCSEL for precise and high-speed wavelength tuning, *Proc. SPIE*, Vertical-Cavity Surface-Emitting Lasers XXVI (2022).

1. Introduction

Vertical-cavity surface-emitting laser (VCSEL) has played a significant role in various industries such as optical communications, consumer electronics and automotive. Its low manufacturing cost, multi-channel design and two-dimensional fabrication on a wafer widened uses of VCSEL and possibility of integration with different materials and devices[1-2].

Tunable micro electro mechanical systems (MEMS) – VCSEL mechanically combined MEMS and VCSEL together. The concept of tunable MEMS-VCSEL is based on direct modulation of the cavity length between two facing mirrors. This tunable light source has been tried to be adapted to the fields of optical communication[3] and spread to curious fields such as spectroscopy and optical coherent tomography (OCT) and light detection and ranging (LiDAR). Frequency modulated continuous wave (FMCW) LiDAR enables more accurate distance measurement than direct time-of-flight (dToF) by continuously tuning lasing wavelength. DToF needs high clock frequency to count time delay of received light. For example, the frequency is over 150 GHz for resolution of 1 mm, which is difficult to achieve. Figure 1 (a) shows optical frequency tuning for FMCW system. Optical frequency is continuously and linearly swept from initial frequency f_0 and increases with known period T and sweep rate γ (up-chirp). The laser is emitted to the object in free space. At the time of τ, the reflected light is collected and optically coupled with the outgoing light, and the beat signal is generated. By calculating the beat frequency Δf, delay time of τ and the distance between the object and FMCW system can be estimated. Measured distance D is expressed as:

$$\mathrm{D} = \frac{c}{2}\tau = \frac{c\Delta f}{2\gamma} \tag{1}$$

where c is the speed of light. Ranging resolution Δd is showed as:

$$\Delta d = \frac{0.89\,c}{f_{BW}} \tag{2}$$

where f_{BW} is frequency bandwidth of tunable light source. The bandwidth is showed as:

$$f_{BW} = c\left(\frac{1}{\lambda_{min}} - \frac{1}{\lambda_{max}}\right) \tag{3}$$

where λ is lasing wavelength, λ_{min} and λ_{max} is minimum and maximum wavelength in tuning range, respectively. Eq. (3) also can be expressed as:

$$f_{BW} = c\left(\frac{1}{\lambda_{cen.} - \frac{\Delta\lambda}{2}} - \frac{1}{\lambda_{cen.} + \frac{\Delta\lambda}{2}}\right) \tag{4}$$

where $\lambda_{cen.}$ is center wavelength and $\Delta\lambda$ is wavelength tuning range. Figure 1 (b) shows the relationship between tuning range of tunable light source and resolution of FMCW LiDAR at the center wavelength of 940 nm. High-resolution distance measurement at the order of sub-millimeter can be possible. For example, with the tuning range of 10 nm, the resolution is theoretically about 80 μm.

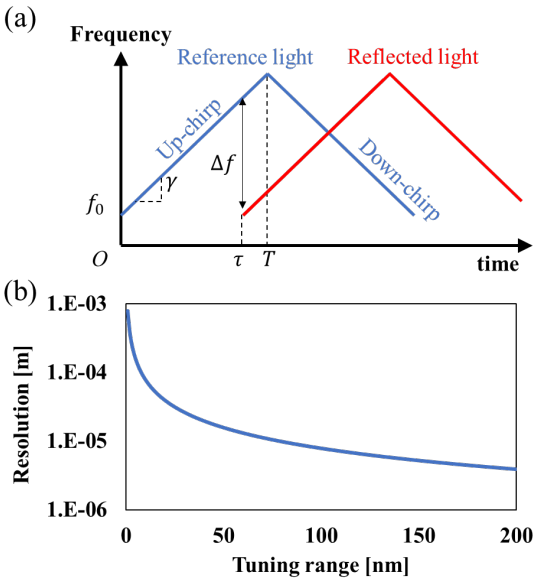

Fig. 1 (a) Modulated optical frequency against time and principle of FMCW LiDAR and (b) relationship between tuning range and distance resolution of FMCW LiDAR at center wavelength of 940 nm.

There are mainly two important conditions for laser source of FMCW LiDAR to satisfy, precise wavelength

control and high-frequency wavelength tuning with higher value of γ. At first, the change of center wavelength $\lambda_{cen.}$ and tuning range $\Delta\lambda$ over the time caused by temperature change and residual stress on actuators should be corrected. It is obvious from Eq. (2) and (4) that the change in $\lambda_{cen.}$ and $\Delta\lambda$ leads to fluctuation of distance resolution. Furthermore, nonlinear wavelength tuning against time causes unstable beat signal and inaccuracy of distance measurement. It has been reported that this nonlinearity gives limited range of resolution[4]. For the latter, at every measurement points the system must wait until the wavelength sweeping is finished. Therefore, the tuning frequency can be the bottleneck for framerate of the system. MEMS tunable VCSELs has possibility of overcoming these challenges.

Since a mirror for laser cavity is fabricated on movable parts on MEMS, the optical characteristics of tunable MEMS-VCSEL directly reflects the types of actuations of MEMS. For example, with linear motion of MEMS and laser cavity design with linear response to change in air-gap enables continuous linear wavelength tuning. For the tuning frequency and range, MEMS structure can have higher-frequency and larger resonant vibration by modifying mechanical and material properties. This modification contributes to the increase in the change of optical cavity length and widening of wavelength tuning range at higher-frequency tuning. These characteristics are decided by the combination of MEMS performance and laser cavity design. For MEMS, there are mainly three types of actuations.

1. Electrostatic MEMS-VCSEL

Electrostatic actuator has been widely used and reported for tunable MEMS-VCSEL[5-10]. Since structure of electrostatic actuator are comparatively simple, integration with other materials or devices can be achieved easier. The displacement of actuator is decided with the balance between electrostatic force and restoring force of MEMS springs. By applying voltage on mirrors, the stable position changes.

To realize high-frequency electrostatic MEMS-VCSEL, three approaches can be chosen, employing low density materials, reducing the thickness of moving parts and increasing applying voltage. The first and second may be challenging. Not only density but some requirements such as mechanical strength, high affinity with semiconductor process and electric property should be satisfied at the same time. Thin and low-mass high contrast grating (HCG) mirror contributed to high-frequency wavelength tuning at about 3 MHz with resonant vibration of MEMS[9], which has higher frequency than conventional tunable MEMS-VCSEL with DBR at 0.698 MHz[10]. The third approach may cause difficulties of obtaining small module and decreased reliability. For the linear actuation, there are drawbacks to overcome such as pull-in effect and nonlinearity of actuation. Since electrostatic force depends on squared value of an applied voltage between MEMS and counterparts, the displacement changes as a function of the squared value, which is not linear to applied voltage. Also, the displacement depends on its initial position. As a result, nonlinearity of MEMS displacement and lasing wavelength occurs, which is difficult to improve linearity by itself without constructing complex optical system and compensating the nonlinearity.

2. Electrothermal MEMS-VCSEL

Electrothermal MEMS converts thermal energy into motion with the thermal expansion and asymmetric deformation. Electrothermal actuators generate large displacements with low energy consumption[11]. Change of lasing wavelength is linear to injection current because deflection of actuator is linear to change of its temperature derived from the injection current. The actuation frequency is relatively slow compared to electrostatic and piezoelectric actuators because change in temperature takes time and this can be the bottleneck of deformation speed. Although electrothermal MEMS at MHz-order are developed with the consideration of dependence of thermal resistant and capacitance on actuators'

dimension[12], their structure and vibration are in-plane and out-of-plane integration with VCSEL device seems challenging.

3. Piezoelectric MEMS-VCSEL

There is fewer report about piezoelectric tunable MEMS-VCSEL[13-16]. Volume change of piezoelectric material is utilized as a source of actuation for a cavity mirror. Piezoelectric materials shrink or expand when voltage is applied on, which is called inverse piezoelectric effect. This effect works linearly to applied voltage and contributes to linear motion of actuators. The shrink of this material is used as the driving force of actuators. Theoretical calculation shows that the piezoelectric material with piezoelectric constant of 590 × 10^{-12} C/N has a hundred times larger energy density than electrostatic actuation, which means larger displacement change per applied voltage can be possible[17]. However, conventional piezoelectric MEMS-VCSEL employed AlGaAs whose piezoelectric constant is much smaller than the value in the calculation described above. Although longer cantilever can compensate the small volume change of AlGaAs, the resonant frequency becomes slower. Therefore, realizing both of wide tuning range and high-frequency tuning at the same time has been difficult. As mentioned above, Table 1 shows the comparison of MEMS-VCSEL based on types of actuators. AlGaAs MEMS-VCSEL has tradeoff between tuning range and frequency.

Table 1 Comparison of MEMS-VCSEL.

	Tuning range	Tuning frequency	Linearity
Electrostatic	○	○	×
Electrothermal	○	×	○
Piezoelectric (AlGaAs)	× (○)	○ (×)	○
Piezoelectric ($Pb(Zr_xTi_{1-x})O_3$)	○	○	○

4. Our concept

To our best knowledge, there are no reports for high linearity of wavelength tuning by itself with designing of MEMS actuator and laser cavity while maintaining high-frequency tuning. We employ $Pb(Zr_xTi_{1-x})O_3$ (PZT) whose volume change is several ten times as large as AlGaAs, which can overcome the tradeoff from conventional piezoelectric material, as showed in Table 1. We aim to realize linear tuning of the center wavelength and high-frequency continuous wavelength sweep and with the combination of the meander and membrane structure. To our best knowledge, this is the first demonstration of PZT MEMS-VCSEL.

In this paper, the integration of PZT MEMS and half-VCSEL is demonstrated. Meander and membrane structures work as adjuster of center wavelength and continuous wavelength sweep over MHz, respectively.

2. MEMS and half -VCSEL Design

The combination between the membrane and meander structures on MEMS is important to adjust the effective cavity length while sustaining high-frequency wavelength tuning. Figure 2 (a) shows the schematic of MEMS. The membrane is located at the center of large stage connected with the meander structure. Dielectric mirror is deposited on the membrane. PZT layers are sputtered on the area that connects the membrane to the large stage. By applying periodic signal on PZT layers near the membrane, the mirror resonates at the specific frequency and generates larger displacement than other frequency range. The lasing wavelength is continuously tuned, and the tuning range depends on the total displacement of the membrane. On the other hand, the meander structure is used to decide the center of the tuning wavelength by adjusting the effective cavity length by actuating with DC-voltage. The details of the meander structure and its principle of motion are discussed later.

Figure 2 (b) shows the cross section of PZT MEMS-VCSEL. MEMS and half-VCSEL are integrated by flip chip bonding with thermal compression. Thermal and mechanical pressure are applied on bonding layers of MEMS and electrodes of half-VCSEL, which causes atomic diffusion without melting and changing the distance of air-gap. On MEMS, adhesive layer and Au bonding layer are patterned by vapor deposition with stainless mask and extended to the edge of MEMS chip. On half-VCSEL, p-electrode and n-electrode are patterned and extended to the edge area of half-VCSEL chip and connected to the electrodes. After bonding process, current is injected from electric pad on MEMS to half-VCSEL through adhesive and bonding layer and electrodes. There are two electrodes on both side of PZT layers to apply voltage on it. Total thickness including adhesive and bonding layers and electrodes is about 1 μm and forms airgap between MEMS and half-VCSEL, which satisfies the requirement for lasing.

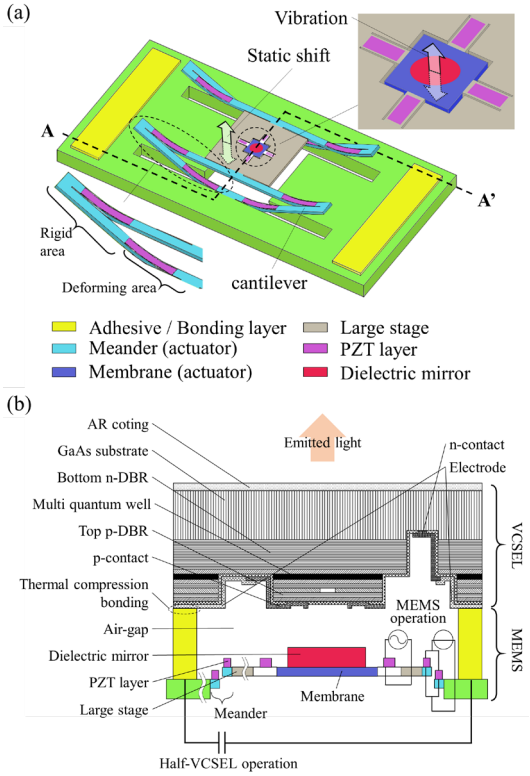

Fig. 2 Schematics of (a) PZT MEMS and (b) cross-section of PZT MEMS-VCSEL after integration along cutting line A-A'.

We used 940 nm bottom-emitting oxide-confined half-VCSEL. Half-VCSEL consists of GaAs substrate, n-AlGaAs distributed Bragg reflector (DBR), InGaAs multiple quantum wells inserted in AlGaAs cavity spacers and top p-AlGaAs DBR with a selective oxidation layer. Combination of p-DBR and external dielectric mirror on the membrane of MEMS works as one mirror with higher reflectivity to construct complete lasing cavity with n-DBR. Output mirror is on the side of n-DBR with lower reflectivity than the dielectric mirror on the membrane of MEMS. The initial air-gap is designed to be 1.25λ.

3. MEMS Performance

Piezoelectric MEMS has different principle of actuation from electrostatic MEMS and has advantage for MEMS-VCSEL. Figure 3 (a) shows schematics of piezoelectric actuator with the meander structure. There is a pair of cantilevers and piezoelectric layer on each cantilever. These two piezoelectric layers are placed to generate displacement x and cancel tilting. At deforming area on the fixed cantilever, piezoelectric layer shrinks with applied voltage and generates tilted angle. This angle is continuous to the rigid area. The rigid area is connected to the other cantilever and the adjacent piezoelectric layer cancel the generated tilted angle by the same magnitude of deformation. Finally, the edge of the second cantilever has the displacement x without changing its tilting angle. The displacement of the meander is showed as:

$$x = \frac{M}{E_p I_p + E_c I_c}\left\{(l_p - \frac{l_c - 2l_j}{2})^2 - \frac{(l_c - 2l_j)^2}{4}\right\} \quad (5)$$

where x is displacement of tip of cantilever, M is bending moment, I is moment of inertia, l is length and E is young modulus. The suffix of p and c and j means piezoelectric material and cantilever and junction between two cantilevers, respectively. Since bending moment is linear to the applied voltage on piezoelectric layers, the displacement also has linearity to the voltage.

Furthermore, the displacement is independent to initial position, which is very advantageous in the situation where the position of the dielectric mirror is shifted by factors such as change of temperature and fabrication process.

Figure 3 (b) shows schematics of electrostatic actuator. Displacement of electrostatic MEMS is calculated with the mechanical parameter and dimension. As described above about electrostatic MEMS, the balance between electrostatic force and restoring force of the spring is showed as:

$$x(g-x)^2 = \frac{\varepsilon_0}{2}\frac{S}{k}V^2 \qquad (6)$$

where x is the displacement of the mirror, g is the initial gap between the plates, ε_0 is dielectric constant of vacuum, S is the area of the mirror, k is the spring constant and V is the applied voltage. On left hand of Eq. (6), restoring force obtains maximum value at $x = g/3$. On the right hand, electrostatic force is proportional to squared value of applied voltage. This equation shows that the relationship between displacement and applied voltage is not linear. Also, the initial gap affects on the control of displacement. By replacing k with $f_0{=}\sqrt{k/m}$, the relationship between the resonant frequency and other parameters is obtained as:

$$x(g-x)^2 \cdot f_0^2 = \frac{\varepsilon_0}{2}\frac{S}{m}V^2 \qquad (7)$$

where f_0 is the mechanical resonance frequency and m is the mass of the mirror. As explained in the previous chapter, it is obvious that there are two options to realize high-frequency resonance frequency while maintaining its displacement, decreasing of mass (reducing density and thickness of material) and increasing of applied voltage. For the former, small volume of mirror and use of materials with lower density contribute to lighter mirror. However, there are some challenges for these options, such as limit of thickness and mechanicals strength of materials. On the other hand, piezoelectric MEMS has different actuation mechanism, such as linearity and independency of displacement on initial position.

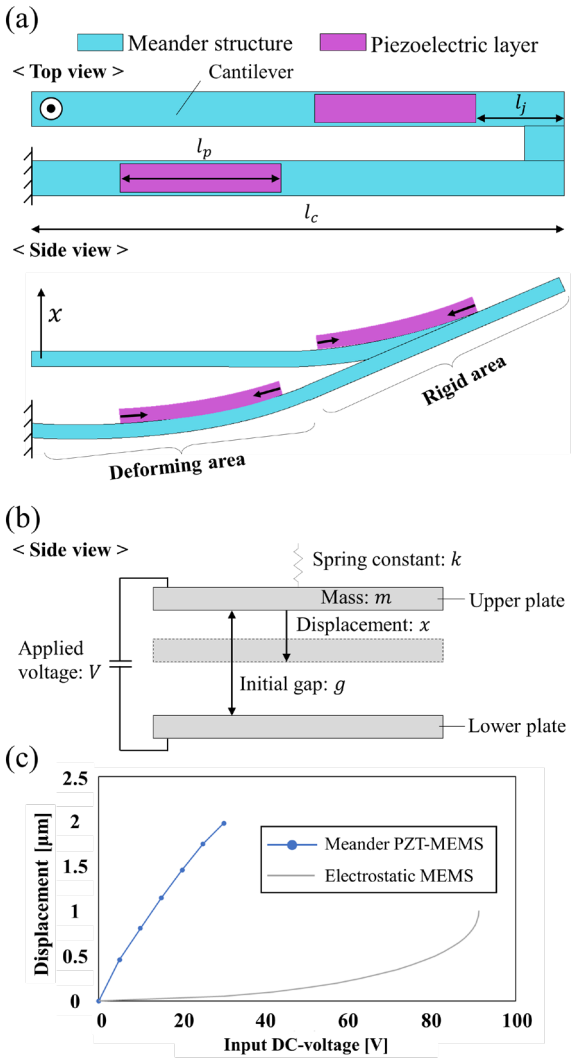

Fig. 3 (a) Schematics of the meander structure from top view and side view, (b) electrostatic actuator and (c) their displacement as the function of applied voltage.

Figure 3 (c) shows the measured displacement of the meander structure with PZT layers and calculated displacement of electrostatic MEMS. The displacement of the meander structure is about 2 μm with applied voltage of 30 V and showed high linearity compared to the calculated electrostatic motion. Coefficient of determination of the meander structure and electrostatic MEMS is 0.992 and 0.876, respectively. With the

calculation on displacement of electrostatic MEMS based on Eq. (7), its resonant frequency is 1 MHz, area of moving plate is 100 μm^2, initial gap is 3 um, length of mirror is 10 μm, thickness is 100 nm, mass of 0.023 pg. The dynamic characteristics of the membrane such as resonant frequency is discussed at the next chapter. From the above results, we found that the combination with the meander and PZT layers can generate large displacement and high linearity to applied DC-voltage without restriction of parameters such as initial air-gap length. This static motion of PZT-MEMS can be employed as the function of adjusting center wavelength of continuous sweep.

4. PZT MEMS-VCSEL Characteristics

1. Measurement setup

Figure 4 (a) shows schematic of connection of MEMS and 4 (b) shows measurement setup. PZT layers on the meander and membrane structure are separately actuated by different channels on the function generator. Channel one (CH1) has DC-voltage output and channel two (CH2) has sinusoidal signal with dc-biased voltage, respectively. MEMS-VCSEL chip is mounted on chip holder, and half-VCSEL is connected to power supply and MEMS is connected to function generator via a connector. PZT layers on the meander structure and membrane are independently driven by different output channel. I-L curve (Injection current vs light output) is obtained by sweeping injection current to half-VCSEL and applying DC-voltage to PZT layers on the meander structure. We have multiple I-L curves depending on the value of DC-voltage on the meander structure. Threshold current is calculated as the slice at the axis of current. Spectra and peak wavelength are measured by spectrum analyzer with DC-voltage to PZT layers on the meander structure. Continuous wavelength tuning range is measured with sinusoidal voltage to PZT layers near the membrane and DC-voltage to those on the meander structure. Spectrum analyzer is set to have long acquisition time so that the sweep of wavelength can be observed. All the measurement is conducted with continuous wave current injection to half-VCSEL at room temperature. Measurement conditions such as DC-voltage, pole, amplitude and frequency for PZT layers on meander and membrane structure and current for half-VCSEL are parameterized by a computer. Emitted light is coupled by objective lens and projected on CCD camera, spectrum analyzer or laser diode tester via optical fiber, which is switchable depending on type of measurement.

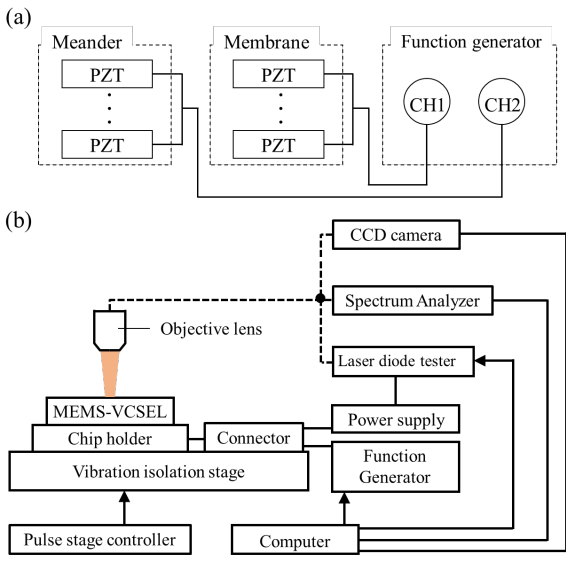

Fig. 4 (a) Schematic of connection for actuation and (b) measurement setup for PZT MEMS-VCSEL.

2. Results

We obtained I-L curve and its dependencies on DC-voltage to PZT layers on the meander structure in continuous wave operation of MEMS-VCSEL, which has an oxide aperture area (S_{OA}) of 60 μm^2. Figure 5 (a) and (b) shows I-L curve and threshold current dependencies on DC-voltage. MEMS design such as dimension of cantilevers and PZT layers differs from those in Figure 3 (c) and showed different displacement range. In Figure 5, the applied voltage to PZT layers on the membrane

structure was set to be 0 V through the measurement. From Figure 5 (a), the maximum optical output was over 0.73 mW with the DC-voltage ($V_{DC\_meander}$) of 2.5 V. The threshold current had tendency of decreasing as the DC-voltage increased in Figure 5 (b). The lowest threshold current was at 2.5 V. We also measured lasing wavelength dependencies on changing DC-voltage to PZT layers on the meander structure.

Figure 5 (c) and 5 (d) shows the tuning range and its linearity and spectra. The operation current ($I_{operation}$) is kept at 10 mA. Since these results are obtained with same sample but different date from Figure 5 (a) and (b), the shift of initial position of the dielectric mirror and disagreement in DC-voltage range to PZT layers on the meander structure occurred. Wavelength tuning range was 8.9 nm and the coefficient of determination reached to 0.992 at room temperature under continuous wave (CW) operation. This linearity is difficult to achieve with non-linear motion of electrostatic MEMS.

When the applied voltage is increased, the dielectric mirror mounted on the membrane moves and shorten the effective cavity length. As a result, lasing wavelength is inverse proportional to the DC-voltage to PZT layers on the meander structure. Lasing wavelength changed from 936.1 nm to 927.2 nm at the range from 2.2 V to 6.2 V. With the help of the meander structure and PZT layers, high linearity of wavelength tuning is achieved. Except nonlinear tuning at the edge of DC-voltage of 2.5 V and 6 V, the measured range of linear tuning was about 6 nm and close to designed value. Wider linear tuning range can be possible by modifying MEMS design and its operation, such as employing lower-mass mirror and piezoelectric material with higher piezoelectric coefficient, increasing in area of PZT layers and applying higher voltage on PZT. The spectra are in transverse multimode oscillation and had wide linewidth, which is supposed to be mainly contributed by two factors, vibration of the meander structure and large oxide aperture on half-VCSEL. Especially for the meander structure, it is designed to create larger displacement with lower voltage and have soft spring, which is easily excited by extrinsic vibration. This vibration generates fluctuation of laser cavity length and lasing wavelength. Stiffer sprig can suppress this fluctuation and multimodal lasing can be suppressed by choosing smaller oxide aperture.

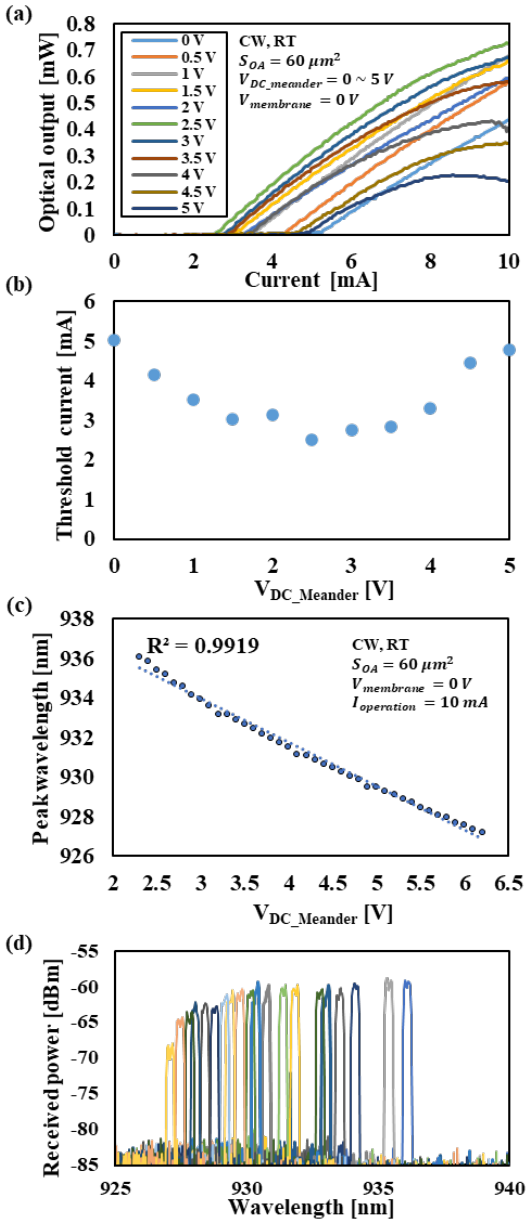

Fig. 5 Static characterization of PZT MEMS-VCSEL. (a) I-L curves, (b) threshold current vs DC-voltage, (c) lasing wavelength vs DC-voltage, (d) lasing spectra.

Finally, we evaluated continuous tuning wavelength dependency on frequency of sinusoidal signal to PZT layers on the membrane structure. Figure 6 shows the tuning range response to input frequency to PZT layers near the membrane. Sinusoidal signal to PZT layers on the membrane structure has peak-to-peak voltage ($V_{pp\_membrane}$) of 20 V and biased voltage ($V_{DC\_membrane}$) of 3.3 V. The operation current ($I_{operation}$) is kept at 10 mA. DC-voltage to PZT layers on the meander structure is set to make the lasing wavelength be in the tuning range during the measurement. The tuning range was 2.98 nm at 1.396 MHz, which is one of the highest-frequency sweep at resonant frequency with DBR on MEMS[10], while HCG reaches to higher resonant frequency of about 3 MHz because of its low-mass mirror[9]. Displacement of the membrane increased because at resonant frequency. However, its tuning range is narrower than the tuning range with DC voltage in Figure 5 because the membrane displacement is smaller than that of the meander actuation. Higher-frequency modulation can be possible with forming low-mass HCG mirror instead of the dielectric mirror. For the linearity of continuous wavelength sweep with the membrane structure, high linearity is expected since PZT layers on the membrane structure also has linear response of volume change to the applied voltage as those on the meander structure.

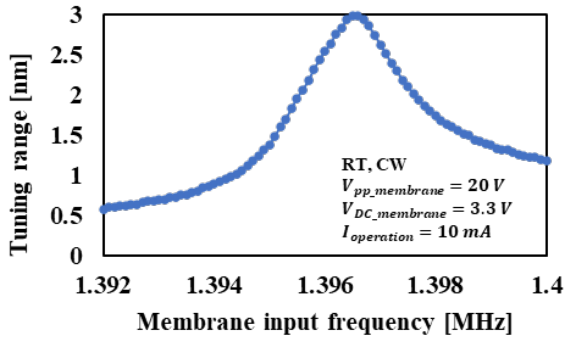

Fig. 6 Tuning range response to MEMS input frequency.

5. Conclusion

In conclusion, we demonstrated 940 nm bottom-emitting tunable MEMS-VCSEL that employed PZT layers as a source of actuators for the first time. Two kinds of actuators, the meander and membrane structure enabled higher linearity and highest frequency of wavelength sweep. The tuning range of lasing wavelength was 8.9 nm with applying DC-voltage to PZT layers on the meander structure at the range from 2.2 V to 6.2 V. Its coefficient of determination between lasing wavelength and applied DC-voltage reached to 0.992, which is difficult to obtain with non-linear motion of electrostatic MEMS-VCSEL. In addition, vibration of membrane realized wavelength tuning range of 2.98 nm with peak-to-peak voltage of 20 V at resonant frequency of 1.396 MHz. This sweep frequency is the highest among DBR MEMS-VCSEL and realized fast operation. More accurate and higher-frequency distance measurement can be expected by improving MEMS structure design.

References

1) K. Iga, F. Koyama, S. Kinoshita: Surface Emitting Semiconductor Lasers, *IEEE J. Quantum Electron.*, Vol. 24, No. 9, pp. 1845-1855 (1988).
2) K. Iga: Surface-emitting laser-its birth and generation of new Optoelectronics Field, *IEEE J. Sel. Top. Quantum Electron.*, Vol. 6, No. 6, pp. 1201-1215 (2000).
3) M. S. Wu et al.: Tunable micromachined Vertical Cavity Surface Emitting Laser, *Electron. Lett.*, Vol. 31, No. 19, pp. 1671-1672 (1995).
4) X. Zhang, J. Pouls, M.C. Wu: Laser frequency sweep linearization by Iterative Learning Pre-distortion for FMCW LIDAR, *Opt. Express*, Vol. 27, No. 7, pp. 9965-9974 (2019).

5) C. Kurokawa et al.: MEMS–VCSEL design method using a diffraction loss map, *OSA Continuum*, Vol. 4, No. 12, pp. 3129-3138 (2021).
6) V. Jayaraman et al.: Rapidly swept, ultra-widely-tunable 1060 nm MEMS-VCSEL, *Electron. Lett.*, Vol. 48, No. 21, pp. 1331-1333 (2012).
7) T. Ansbaek et al.: Resonant MEMS tunable VCSEL, *IEEE J. Sel. Top. Quantum Electron.*, Vol. 19, No. 4 (2013).
8) T. Yano et al.: Wavelength modulation over 500 khz of micromechanically tunable INP-based VCSELs with Si-MEMS technology, *IEEE J. Sel. Top. Quantum Electron.*, Vol. 15, No. 3, pp. 528-534 (2009).
9) Zhou, Y., Huang, M.C., Chang-Hasnain, C.J.: Tunable VCSEL with ultra-thin high contrast grating for high-speed tuning, *Opt. Express*, Vol. 16, No. 18, pp. 14221-14226 (2008).
10) Cole, G.D et al.: Short-wavelength MEMS-tunable VCSELs, *Opt. Express*, Vol. 16, No. 20, pp. 16093-16103 (2008).
11) A. Potekhina, Changhai. W: Review of electrothermal actuators and applications, *Actuators*, Vol. 8, No. 4, p. 69 (2019).
12) A. Rahafrooz, A. Hajjam, S. Pourkamali: Thermal actuation of high frequency micromechanical resonators, *2009 IEEE International SOI Conference* (2009).
13) G. Piazza et al.: Design of a monolithic piezoelectrically actuated microelectromechanical tunable vertical-cavity surface-emitting laser, *Opt. Lett.*, Vol. 30, No. 8, pp. 896-898 (2005).
14) M. C. Y. Huang et al.: Demonstration of piezoelectric actuated GaAs-based MEMS Tunable VCSEL, *IEEE Photon. Technol. Lett.*, Vol. 18, No. 10, pp. 1197-1199 (2006).
15) Kan Bun Cheng et al.: Monolithic integration of piezoelectric cantilever in tunable VCSEL, *IEEE/LEOS International Conference on Optical MEMS and Their Applications Conference* (2006).
16) Huang, M.C et al.: Monolithic integrated piezoelectric MEMS-Tunable VCSEL, *IEEE J. Sel. Top. Quantum Electron.*, Vol. 13, No. 2, pp. 374-380 (2007).
17) H. Toshiyoshi: Seiden maikuro akuchuetā no kudō kikō to sekkei genkai (Drive mechanism and design limits of electrostatic microactuators) [Translated from Japanese], *J. the Society of Instrument and Control Engineers*, Vol. 42, No. 1, pp. 18-23 (2003).